https://doi.org/10.17221/24/2025-SWR

The role of ground heat flux in estimating evapotranspiration by the Penman-Monteith method on mountain meadow

Michal Dohnal[1], Jana Votrubová[1], Rebeka Mazúchová[1], Miroslav Tesař[2]*

[1]Faculty of Civil Engineering, Czech Technical University in Prague, Prague, Czech Republic
[2]Institute of Hydrodynamics of the Czech Academy of Sciences, Prague, Czech Republic

**Corresponding author michal.dohnal@cvut.cz*

Citation: Dohnal M., Votrubová J., Mazúchová R., Tesař M. (2025): The role of ground heat flux in estimating evapotranspiration by the Penman-Monteith method on mountain meadow. Soil & Water Res., 20: 265–273.

Abstract: Ground heat flux (*G*) is often an overlooked component of the surface energy balance, and its accurate determination remains challenging. In the present study, the accuracy of various *G* estimation methods is examined using long-term measurements from the Central European mountain meadow. The impact of different *G* approximation on calculated evapotranspiration by the Penman-Monteith method (*ET*) is analysed. Soil heat flux measurements and surface temperature data were used to determine *G*, while net radiation was used to approximate *G*. Neglecting *G* led to an overestimation of *ET* in the daily timestep. On the contrary, the FAO-recommended hourly approximation overestimated *G*, underestimating *ET*. Site-specific calibrations of *G* prediction models improved their accuracy. For daily average *G*, as well as for hourly average *G*, simple constant parameter models (i.e., models including a single parameter specifying the fraction of net radiation directly) provide satisfactory accuracy of *ET* evaluation. However, in an hourly timestep, net radiation fails as a predictor of *G* shortly after sunrise and before sunset. The findings emphasise the importance of considering *G* in *ET* calculations and the need for site-specific calibrations of *G* estimation models.

Keywords: evapotranspiration of grass; Penman-Monteith equation; sandy loam texture; soil heat flux; soil temperature

The ground heat flux (*G*), is part of the surface energy balance and plays an essential role in evapotranspiration. However, *G* is often neglected or ignored in energy balance calculations and evapotranspiration estimates (Allen et al. 1998; Campbell & Norman 1998; Li et al. 2023). Less often, ground heat flux is approximated or estimated using models or relationships derived from limited observations (e.g., Irmak et al. 2011; Liu 2022). Much less frequently, this flux is directly measured (e.g., Sun et al. 2022). This is primarily due to the difficulty of accurately measuring the heat flux to the soil. The absence of measurements of ground heat flux, or a crude approximation of it, can lead to inaccuracies in the quantification of energy balance and estimation of evapotranspiration, with implications in the field of soil biology and ecosystem ecology.

G plays a critical role in regulating surface temperatures and influencing local microclimate patterns (Sauer & Norman 1995). Soil temperature, directly influenced by *G*, governs microbial activity, nutrient cycling, and decomposition rates (Smith et al. 2018). Uncertainty in the determination of *G* (Zawilski 2022) may bias our understanding of soil biogeochemical processes.

Supported by the Student Grant Competition programme of the Czech Technical University in Prague, Grant No. SGS23/153/OHK1/3T/11.

https://doi.org/10.17221/24/2025-SWR

Given the challenges of direct *G* measurements, numerous methods have been developed to approximate its value at the local scale. Empirical models utilise relationships between *G* and other more easily measurable variables such as net radiation or vegetation cover (e.g., Tasumi et al. 2005). However, the accuracy of these models can vary significantly depending on the specific site conditions and the quality of input data (Ochsner et al. 2006).

The present study aims to evaluate the accuracy of various methods for estimating ground heat flux and to assess the impact of *G* on evapotranspiration calculations. By using long-term soil heat flux measurements and surface temperature data, the study analyses the performance of selected approaches for determining *G*. Special attention is paid to the demonstration of the effect of considered neglecting and approximations of *G* on *ET* modelling and water balance calculations. Additionally, site-specific calibrations of different *G* prediction models are presented.

MATERIAL AND METHODS

Experimental site. The experimental meteorological station Liz is located in a mountain meadow of Bohemian Forest, Czech Republic (49°4.18562'N, 13°40.92510'E, Figure 1). The station is situated at an altitude of 830 m, it covers approximately 816 m^2, with the majority of its area characterised by permanent grassland and interspersed with sections of mosses. The mean annual precipitation is 861 mm and the mean annual air temperature is 6.3 °C. The soil is a Cambisol with sandy loam texture developed on biotite paragneiss bedrock.

Meteorological monitoring 2 m above ground includes air temperature and air humidity (Vaisala HMP45), wind speed (Vaisala anemometers WA151), air pressure (Setra Barometric Pressure Sensor), and radiation (CNR1 Net Radiometers, Kipp & Zonen). Soil thermal condition observation includes soil temperature (platinum temperature sensor Pt100-A, Fiedler AMS) and soil heat flux (HFP03), both 5 cm below the surface. A pair of heat flux sensors is installed approximately 1 m apart. The expected typical accuracy of heat flux measurement in soil is within −15% to +5% (HFP03, Hukseflux Thermal Sensors).

Data is collected in ten-minute timestep. Radiation sensors are removed during winter. Vegetation seasons (part of the year from April to October) from 2017 to 2021 were used for the analysis (Table 1). To ensure comparability among the years, the season was set so that observations are equally available in each year under study. Specifically, from April 23 to October 9.

Calculation of evapotranspiration. Evapotranspiration intensity of vegetation, *ET* (m/s), was estimated by the Penman-Monteith equation (Monteith 1965):

$$ET = \frac{1}{\lambda \rho_w} \frac{\delta (R_n - G) + \rho_a c_p \frac{p_{vs} - p_v}{r_a}}{\delta + \gamma \frac{r_a + r_s}{r_a}} \quad (1)$$

where:

λ – the latent heat of vaporization (J/kg);

ρ_w – the density of water (kg/m^3);

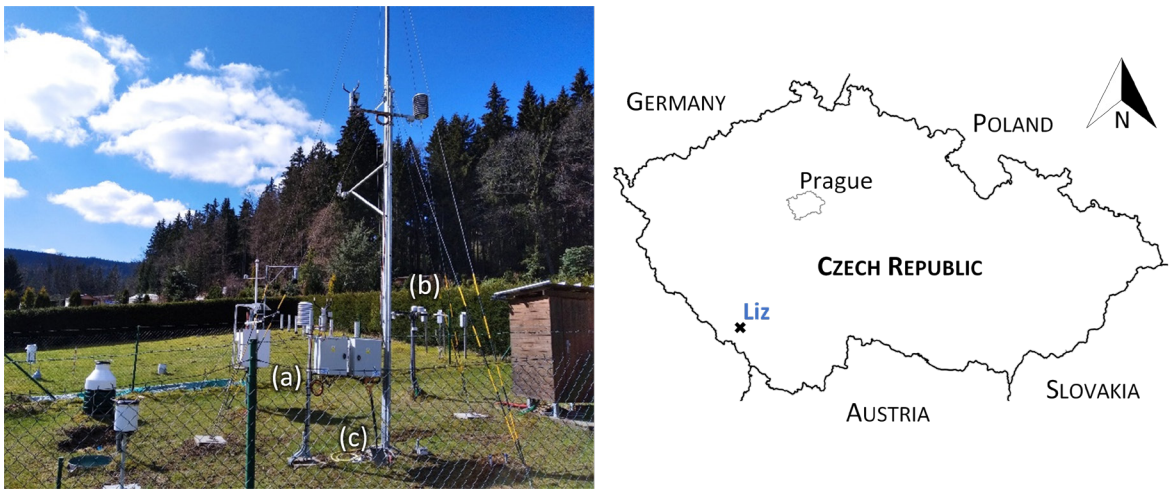

Figure 1. The layout of the meteorological station Liz

Position of heat flux sensors (a), 4-component net radiometer (b), location of soil temperature probes (c)

https://doi.org/10.17221/24/2025-SWR

Table 1. Basic hydrometeorological variables for individual seasons; the length of the seasons is the same in all years, the basis is determined by the availability of radiation measurements (i.e., April 23 to October 9); evapotranspiration values are calculated hourly using measured ground heat flux (G), negatives are ignored

Season	T (2 m) (°C)	r (%)	R_n (W/m^2)	p_a (hPa)	u (m/s)	H_s (mm)	ET (mm)
2017	13.9	72.1	100.3	921.3	0.56	396.7	465.3
2018	15.2	71.7	99.6	922.5	0.54	448.2	469.6
2019	14.1	72.4	96.5	921.2	0.55	387.5	450.0
2020	13.5	73.3	99.3	920.8	0.54	547.3	453.2
2021	13.3	74.1	104.5	921.5	0.43	635.3	456.6

T (2 m) – air temperature at 2 m; r – relative air humidity; R_n – net radiation; p_a – barometric pressure; u – wind speed at 2 m; H_s – rainfall depth; ET – evapotranspiration

δ – the slope of saturated vapour pressure curve (Pa/K);
R_n – the net radiation (W/m^2);
G – the ground heat flux (W/m^2);
ρ_a – the air density (kg/m^3);
c_p – the specific isobaric heat capacity of air (J/kg/K);
$(p_{vs} - p_v)$ – the vapour pressure deficit of air (Pa);
γ – the psychrometric constant (Pa/K);
r_a – the aerodynamic resistance (s/m);
r_s – the vegetation bulk surface resistance (s/m).

The second fraction represents the evaporation-related latent heat flux (W/m^2). The first fraction serves to convert the energy flux into the volumetric flux of water.

Determination of the ground heat flux. The soil heat flux is measured 5 cm below the surface (installation of the soil heat flux sensors 5 cm below the surface is required by the manufacturer to avoid disturbance). To obtain the ground heat flux, i.e., soil heat flux at the soil surface, additional calculation is needed. The calorimetric approach is used as suggested by the manufacturer (Hukseflux Thermal Sensors 2006):

$$G = G_H + \left[\frac{(T_2 - T_1)C_s\, d}{t_2 - t_1}\right] \quad (2)$$

where:
G_H – the heat flux (W/m^2) measured by the Hukseflux sensor in the soil;
$T_2 - T_1$ – the change of the overlying soil layer temperature (K) during the measurement interval $t_2 - t_1$ (s);
C_s – the volumetric heat capacity of the soil (J/m^3/K);
d – the depth of the sensor installation (m).

G was determined in an hourly time step. The value of the volumetric heat capacity was taken as an average of seven consecutive measurements by ISOMET 2114 (Applied Precision Ltd., Slovakia), C_s = 1.919 10^6 J/m^3/K. The value of volumetric heat capacity was considered to be constant. Daily G values were calculated as the average of hourly G values.

Since the heat storage change within the overlying soil layer (the second additive term in Equation (2)) affects the calculated heat flux at the soil surface significantly, various approximations of overlying soil layer temperature were considered:

Variant 1:

$$T = 0.75T_{-5cm} + 0.25T_{rad} \quad (3a)$$

Variant 2:

$$T = 0.5T_{-5cm} + 0.5T_{rad} \quad (3b)$$

Variant 3:

$$T = T_{-5cm} \quad (3c)$$

where:
$T_{-5\,cm}$ – the soil temperature measured at a depth of 5 cm (K);
T_{rad} – the effective ground temperature calculated from radiometer measurement (K).

Assuming that ground behaves like a perfect blackbody, the irradiance of the ground (measured with the downward-facing pyrgeometer part of CNR1, i.e. CG3 sensor, Kipp & Zonen) can be used to calculate an effective ground surface temperature T_{rad} (K):

$$T_{rad} = \left(\frac{L_G}{\sigma}\right)^{\frac{1}{4}} \quad (4)$$

https://doi.org/10.17221/24/2025-SWR

where:
L_G – the outgoing long wave radiation (W/m^2);
σ – the Stefan-Boltzmann constant, σ = 5.6704 10^{-8} W/m^2/K^4.

Standard approximation of ground heat flux in P-M equation. It is often stated that G can be neglected in the daily time step ET calculation (Seguin & Itier 1983; Allen et al. 1998). This corresponds to the assumption that the cumulative heat flux to the soil per day is zero.

Hourly-resolution G can be approximated as a fraction of R_n. Specifically, 0.1 R_n during daylight periods and 0.5 R_n during night-time periods (Burridge & Gadd 1977). Burridge and Gadd (1977) is a representative of approaches considering a constant proportion of R_n during vegetation season and is recommended by FAO Irrigation and Drainage Paper No. 56 (Allen et al. 1998).

Tested site-specific models of the ground heat flux. Site specific calibration of various models estimating G from measured R_n was conducted. All can be generalised by the following expression:

$$G = aR_n + c_G \tag{5}$$

where:
a (–), c_G (W/m^2) – parameters that may or may not be variable in time.

For the daily average G, three models are considered, two of which introduce variability of the parameters throughout the vegetation season. Constant-a model assumes constant site-specific a and c_G = 0. Sine-a model combines c_G = 0 with a that varies sinusoidally. Finally, the sine-c_G model assumes a combination of constant a and sinusoidally variable c_G. The sinusoidal variability is described as follows:

$$X = X_{min} + \frac{X_{max} - X_{min}}{2}\left(1 + \cos\left(2\pi\frac{DOY - D_{max}}{365}\right)\right) \tag{6}$$

where:
X – standing for a or c_G;
X_{min}, X_{max} – maximum and minimum values of the parameter;
DOY – the day of year serial number;
D_{max} – the serial number of the day when X_{max} applies.

For hourly average G, two models are considered, both assuming that c_G in Equation (5) is zero and the parameter a varies during the day. First concept assumes separate constant a values for daytime and nighttime (equivalent to above mentioned Burridge and Gadd 1977). Eventually, a model with a varying linearly during the daytime is tested (linear-a model):

$$a = a_{sr} + \frac{t - t_{sr}}{t_{ss} - t_{sr}}(a_{ss} - a_{sr}) \qquad \text{for } t \in \langle t_{sr}, t_{ss} \rangle \tag{7}$$

$$a = a_{night} \qquad \text{for } t \notin \langle t_{sr}, t_{ss} \rangle \tag{8}$$

where:
t – the time (h);
sr – sunrise;
ss – sunset.

The three parameters a_{sr}, a_{ss}, and a_{night} are a values effective at sunrise, sunset, and nighttime, respectively.

Model calibration was conducted using data from the year 2021 by minimization of the root mean square error (RMSE) of the G estimates.

Performance of all introduced G-approximation methods was assessed not only by comparing the estimated G values with measured G values, but also by examining the errors of ET estimates associated with using the G approximations instead of the measured G.

RESULTS

Uncertainty in the determination of ground heat flux. The evaluation of the ground heat flux, G, combines the conductive heat flux measured at the depth of 5 cm and the heat storage change within the overlying soil layer (Equation (2)). Calculation of the heat storage change relies on evaluation of the soil temperature changes in the soil layer above the heat flux sensors. Relevant available data describe the temperature at the soil layer boundaries, namely the soil temperature measured at the sensor depth, $T_{-5\ cm}$, and the soil surface temperature estimated based on the measured longwave radiation, T_{rad} (Equation (4)). In the present study, three variants of combining the layer boundaries temperatures were considered (Equation (3)). Their effect on the calculated ground heat flux at the soil surface is illustrated in Figure 2.

Comparison of the hourly G during sunny days, Figure 2B, demonstrates that increasing the weight of the surface temperature in the heat storage calculation enhances the swiftness of the estimated G response to the net radiation changes. A similar

https://doi.org/10.17221/24/2025-SWR

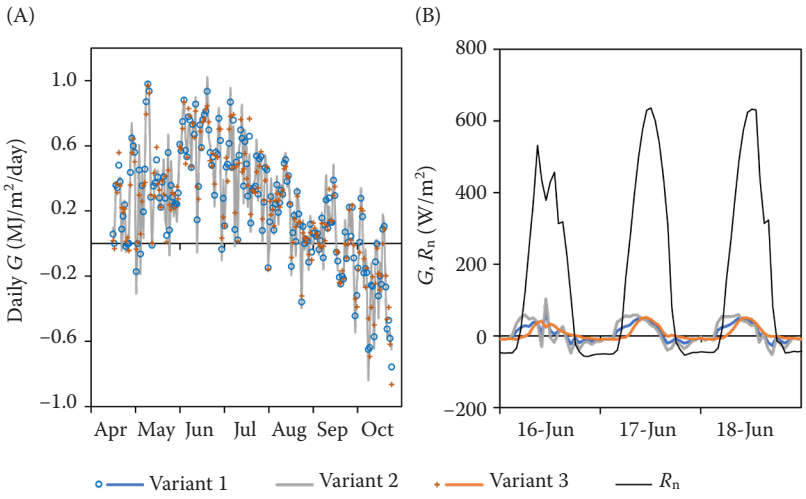

Figure 2. Determination of soil heat flux at surface level; comparison of variants combining the layer boundaries temperatures: daily G in vegetation season 2021 (A), hourly G during three consecutive sunny days in June (B)
G – ground heat flux; R_n – net radiation

effect is apparent in the daily average G variations, Figure 2A, in which case increased day-to-day variability is obtained. The daily G values estimate differ by up to 0.4 MJ/m²/day, which, as latent heat, would relate to evaporation of approx. 0.16 mm of water. However, the cumulative difference over the whole vegetation season is negligible (0.6 MJ/m², which is 1.2% of the cumulative ground heat flux only).

Variant 1 of the G calculation was chosen for further analysis. The selection was based on the comparison between hourly G and R_n variation, e.g., Figure 2B. Consideration of the surface temperature changes is essential to obtain G that mimics reasonably the soil temperature changes. Still, based on the expected temperature profiles within the surface layer we believe that the average temperature within this soil layer is better described when the relative weight of the surface temperature in the calculation is reduced (Equation (2a)).

Effect of neglecting G in daily ET assessment. When evapotranspiration is evaluated in a daily time step, the average daily ground heat flux is usually considered zero, i.e., neglected. As can be seen in Figure 2A, this assumption is rarely met. It is obvious that during the main vegetation season, from May to August, positive values of G prevail. This is because the heat flux into the soil during the daytime is significant, and most of the heat accumulated in the soil doesn't radiate back into the atmosphere during the night. It creates a positive imbalance in the soil heat flux, and the assumption of zero cumulative ground heat flux per day notably incorrect. Consequently, neglecting G induces an overestimation of evapotranspiration.

In Figure 3, the evapotranspiration difference induced by neglecting G is presented (ΔET, daily values during the vegetation season 2021). It can be seen that the evapotranspiration difference induced by neglecting G is smaller than the equivalent of G expressed as evaporation (G = 1 MJ/m²/day as seen in Figure 3A, which would, as latent heat, relate to evaporation of 0.4 mm/day). This is due to the fact that the Penman-Monteith method considers not only the available energy but also the effect of wind and air humidity on the evaporation process. The available energy is consumed by evaporation and convective sensible heat flux into the atmosphere. Consequently, different ΔET values can be related to the same G. This difference is mainly due to the temperature dependence of the slope of the saturated vapour pressure curve δ. More specifically, $\Delta ET/(\Delta G/\lambda\rho_w)$ varies between

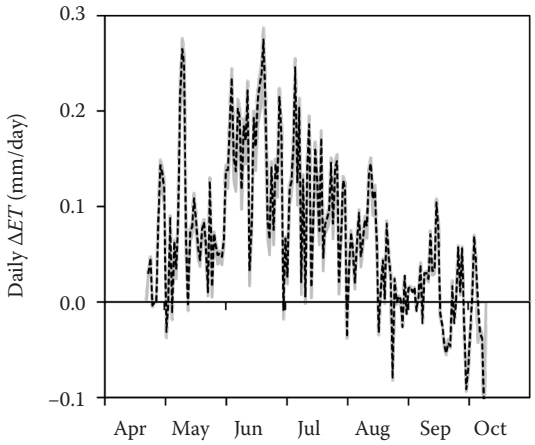

Figure 3. Evapotranspiration difference induced by neglecting ground heat flux (G) in daily evapotranspiration (ET) assessment during the vegetation season 2021; the shaded area reflects G equal to the limits of ranges defined by the sensor accuracy

https://doi.org/10.17221/24/2025-SWR

Table 2. Comparison of daily evapotranspiration (*ET*) calculated using either neglected or measured ground heat flux (*G*); values in brackets are obtained considering limits of ranges of likely *G* assuming the sensor accuracy

Season	Root mean square error (mm/day)	Seasonal cumulative difference (mm) (%)
2017	0.124 (0.108; 0.129)	14.0 (11.8; 14.9) (–16%/+7%)
2018	0.113 (0.098; 0.116)	13.1 (10.7; 13.7) (–18%/+5%)
2019	0.125 (0.108; 0.129)	13.7 (11.8; 14.8) (–14%/+8%)
2020	0.105 (0.092; 0.109)	11.9 (10.0; 12.7) (–16%/+6%)
2021	0.106 (0.093; 0.110)	12.1 (10.2; 12.8) (–16%/+6%)

0.4 at the air temperature of 0 °C and 0.8 at the air temperature 35 °C.

At our experimental site in years 2017 and 2021, the cumulative effect of neglecting *G* in daily-step *ET* assessment was between 11 and 14 mm per vegetation season (Table 2). This represents 1.5 % of the mean annual precipitation or 3 % of *ET* at the site.

Effect of standard *G* approximation in hourly *ET* assessment. Calculating *ET* in hourly time steps using standard *G* approximation as either 0.1 R_n (daylight) or 0.5 R_n (night-time) generates an overall *ET* underestimation, which is a direct consequence of overestimating daytime *G* (Figure 4). The seasonal cumulative difference is about –19 mm, with the largest cumulative difference of –22 mm in the hydrologically above-average season of 2021 (Table 3). During all examined seasons, *ET* is underestimated for approximately 60% of the daytime. Differences (ΔET) are evenly distributed throughout the vegetation season (not shown here), with the largest differences reaching –0.09 mm/h.

Hourly G/R_n variation analysis. Although the above approximations of *G* provide acceptable accuracy of *ET* estimation, site-specific *ad hoc* calibration is usually recommended (e.g., Purdy et al. 2016). To gain insight into the potential of using R_n to estimate *G*, the measured G/R_n ratio and its changes during the day, as well as throughout the vegetation season, were investigated (Figure 5).

The nighttime G/R_n is quite stable over time and is approximately equal to 0.2. During the day, the G/R_n value decreases from 0.4 in the morning to 0.05 at midday, and –0.15 in the afternoon. The G/R_n ratio is extremely unstable in the morning. The drop to negative values is due to *G* changing its direction earlier than R_n

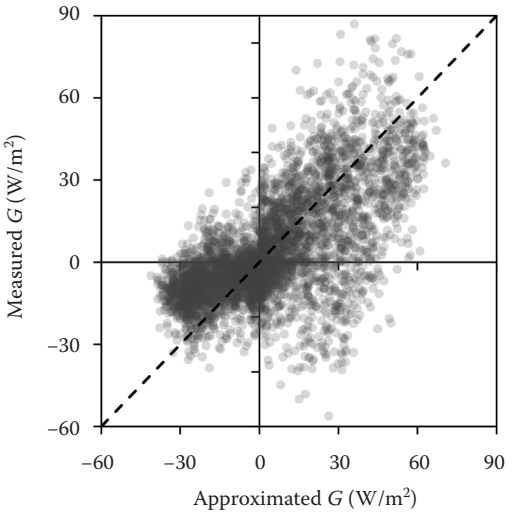

Figure 4. Calculated vs. measured ground heat flux (*G*) in an hourly time step in season 2017; calculation was done as a part of net radiation (R_n) (Burridge & Gadd 1977) dashed line shows the equivalence of calculated and measured hourly *G*

Table 3. Comparison of hourly evapotranspiration (*ET*) calculated using either estimated Burridge and Gadd (1977) or measured ground heat flux (*G*); values in brackets are obtained considering limits of ranges of likely *G*, assuming the sensor accuracy

Season	Root mean square error (mm/h)	Seasonal cumulative difference (mm) (%)
2017	0.015 (0.014; 0.015)	–17.6 (–16.5; –20.0) (–6%/+14%)
2018	0.016 (0.015; 0.016)	–18.0 (–17.0; –20.3) (–5%/+13%)
2019	0.013 (0.013; 0.014)	–16.4 (–15.5; –18.8) (–6%/+14%)
2020	0.014 (0.014; 0.014)	–20.6 (–19.8; –22.5) (–4%/+9%)
2021	0.015 (0.015; 0.015)	–22.3 (–21.4; –24.2) (–4%/+9%)

https://doi.org/10.17221/24/2025-SWR

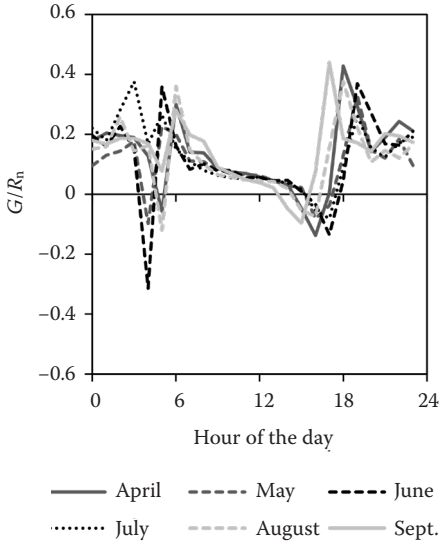

Figure 5. Daily variation of G/R_n obtained for individual months in 2021 by linear regression without the intercept term of the hourly G vs. R_n data
G – ground heat flux; R_n – net radiation

(typically a difference of 1 hour). Moreover, as the value of the increasing R_n becomes close to zero, G/R_n tends to infinity. A similar transition takes place in the afternoon and evening, but it is stretched over a longer time period. The afternoon negative G/R_n values are due to negative G while R_n stays positive (starting typically 4 hours before sunset). Then, during the last hour before sunset, R_n changes direction, while approaching zero and causing extreme G/R_n values. The variability of G/R_n daily course among months (Figure 5 – June vs September) reflects mainly the changes of the daylight duration at the site.

Daily *G* models. Concerning the daily average G, first a constant G/R_n fraction was assumed – a constant-a model (Equation (5)). The optimised a value is 0.034, with root mean square error (RMSE) criterion 2.92 W per m^2. The method of Tasumi (2005) that acknowledges the influence of vegetation cover on the heat transferred into the soil results for relatively dense clipped grass (with constant LAI = 4) in considerably higher value of 0.072 (with RMSE = 5.06 W/m^2).

Comparing the estimated and measured values overall, the constant-a model underestimates the extent of variability, both daily and seasonal (Figure 6). At the beginning of the vegetation season, the model fails to capture the character of daily variation. The change of R_n is not a good predictor of whether G will increase or decrease. At the end of summer (in our case, from the end of August), the model's inability to produce negative G values while positive R_n is observed becomes a clear disadvantage.

Consequently, a seasonally sinusoidally variable value of a was introduced (optimisation indicates annual sinusoidal variation between –0.058 on December 15 and 0.047 on June 16, with RMSE equal to 2.36 W/m^2). This approach (sine-a model) leads to improved predictions in terms of seasonal variability, capturing the switch to negative G in autumn (a becomes negative on September 9). This is accompanied by the inability of the model to mimic the extent of the daily variability in the vicinity of this switching date. However, the original constant-a model fails during this time period as well, overestimating G systematically.

Alternatively, the ability of the model to reproduce seasonal variability can be improved by introducing a seasonally variable additive term, c_G (optimisation indicates annual sinusoidal variation between –5.307

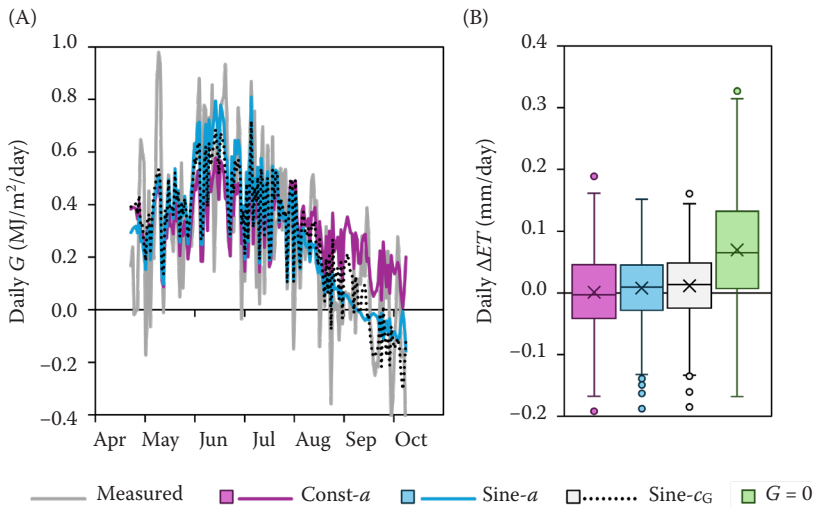

Figure 6. Comparison of the daily G values measured or estimated using various models: seasonal variations of daily G in vegetation season 2021 (A), daily ET estimate errors (ΔET) associated with various daily-G models as obtained over the five vegetation seasons 2017–2021 (B)
G – ground heat flux; ET – evapotranspiration; a, c_G – parameters that may or may not be variable in time

https://doi.org/10.17221/24/2025-SWR

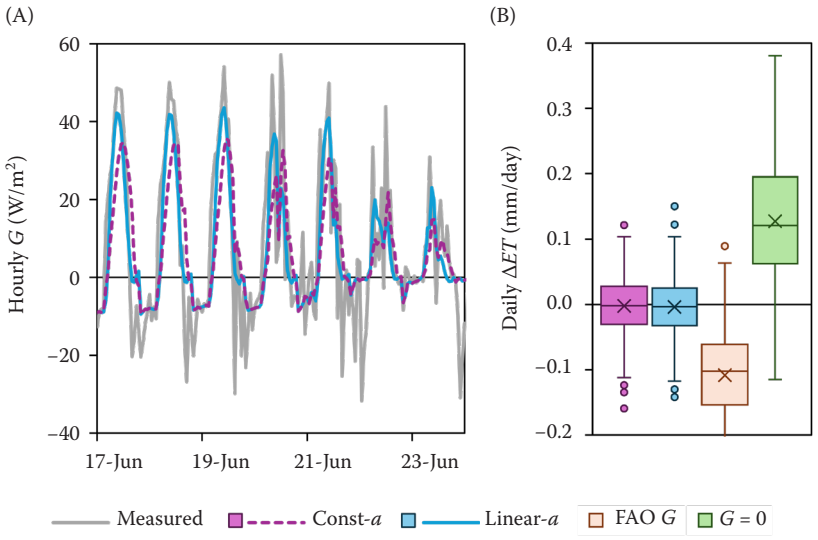

Figure 7. Comparison of the hourly *G* values measured or estimated using various models: several-day variations of hourly *G* in June 2021 (A), daily sums of hourly calculated *ET* estimate errors (Δ*ET*) associated with various hourly-*G* models as obtained over the five vegetation seasons 2017–2021 (B)

G – ground heat flux; *ET* – evapotranspiration; *a* – parameter that may or may not be variable in time

on December 10 and 0.860 on June 11, combined with constant a = 0.036, RMSE = 2.31 W/m^2). This approach combines advantages of the earlier discussed models. The overall ability to predict the measured *G* values is similar to the sine-*a* model.

When comparing the effect of various *G* models on *ET* prediction (Figure 6B), it becomes obvious that the improvement in capturing *G* achieved using a more complicated model does not have to be reflected in an improved *ET* estimate. Specifically, using the sine-c_G model does not provide better daily *ET* estimates than using the sine-*a* model. This is due to the fact that while the sine-c_G model improves *G* predictions significantly at the end of the vegetation season (September, October), it is actually worse during the months with the highest evapotranspiration drive (June and July). It is clear that the simple constant-*a* model provides a clear improvement compared assuming *G* = 0. Considering more complicated *G* models does not contribute much to the accuracy of *ET* evaluation.

Hourly *G* models. When hourly *G* is considered, different fraction of R_n during daytime and overnight is usually considered. In our case, optimised values of *a* are 0.054 for daytime and 0.177 overnight (RMSE = 14.37 W/m^2).

Our observations, as presented in Figure 5, indicate that applying time-dependent *a* during daytime could improve the *G* estimate. In our case, when considering linear daytime variation of *a*, optimisation led to a = 0.155 at sunrise and a = –0.050 at sunset, and constant a = 0.177 during night (RMSE = 12.98 W/m^2). As can be seen in Figure 7A, this simple model leads to a clear improvement in capturing the character of daily *G* variations. However, the afternoon *G* drop to negative values is not represented sufficiently. Although a slightly better approximation in terms of the RMSE criterion can be obtained when assuming more complicated expressions to describe *a* daytime variation, the extent of the improvement does not warrant the increased model complexity. Actually, it is obvious that four hours before sunset, R_n becomes an increasingly poor predictor of *G*.

The effect of various hourly *G* approximations on the calculated *ET* is shown in Figure 7B. The errors of the daily sum of hourly calculated *ET* are presented. It can be seen that at our site, the standard *G* approximation does not produce a greatly better *ET* estimate compared to the case of neglecting *G*. As expected, a considerable improvement is provided by the site-specific *G* models. However, the improvement achieved with a more complex linear-*a* model compared to a simple constant-*a* model is negligible.

CONCLUSION

The present study deals with the evaluation of soil heat flux measurements, its conversion to the surface, and tests the quality of the most used methods for estimating *G* on the mountain meadow. At the same time, it offers a discussion of the results of various site-specific models estimating *G* from measured R_n calibrated on the available data.

The involvement of surface soil temperature proved critical for determining the heat flux to the soil at the surface level. The surface temperature, together with the soil temperature at the place of a sensor installation, provides a better approximation of the

https://doi.org/10.17221/24/2025-SWR

temperature profile in the soil above the sensor. Of those tested, the best option was the one that describes the average temperature in the soil volume above the sensor with a quarter of the relative weight of the surface temperature in its calculation.

The assumption of zero cumulative heat flux to the soil per day during the vegetation season at the latitude of the experimental site is clearly incorrect. Consequently, neglecting *G* leads to an overestimation of evapotranspiration. At the study site, it represents approximately 2% of the average annual precipitation. In contrast, the approximation *G* for the hourly time-step recommended in the FAO methodology overestimates *G* for over 60% of the daytime. This leads to an underestimation of the calculated *ET*. Both main results remain valid even when the accuracy declared by the sensor manufacturer is considered and incorporated into the calculation of ground heat flux and subsequently *ET*. On the other hand, the study is conducted on a single soil type at a mid-latitude location, and site-specific calibration of the *G* prediction model is highly recommended.

In our case, site-specific calibrations of different *G* prediction models yielded interesting results. In the daily time-step, the approach using seasonally sinusoidally variable parameter leads to improved predictions in terms of seasonal variability and satisfactorily describing change to negative *G* in autumn. In sub-daily time-step, it is important to note that R_n becomes a poor predictor of *G* during few hours before the sunset. Results also indicate that applying time-dependent parameter during daytime could improve the *G* estimate.

Acknowledgements. Soil heat flux and meteorological data were available through the courtesy of the Institute of Hydrodynamics of the Czech Academy of Sciences. The student co-author, Rebeka Mazúchová, was supported by the Student Grant Competition programme of the Czech Technical University in Prague, Grant No. SGS23/153/OHK1/3T/11.

REFERENCES

Allen R.G., Pereira L.S., Raes D., Smith M. (1998): Crop Evapotranspiration: Guidelines for Computing Crop Water Requirements. Rome, FAO.

Burridge D.M., Gadd A.J. (1977): The Meteorological Office Operational 10-level Numerical Weather Prediction Model. Scientific Paper – Meteorological Office. Bracknell, British Meteorological Office.

Campbell G.S., Norman J.M. (1998): An Introduction to Environmental Biophysics. Springer.

Irmak A., Singh R.K., Walter-Shea E.A., Verma S.B., Suyker A.E. (2011): Comparison and analysis of empirical equations for soil heat flux for different cropping systems and irrigation methods. Transactions of the ASABE, 54: 67–80.

Li T.L., Schiavo M., Zumr D. (2023): Seasonal variations of vegetative indices and their correlation with evapotranspiration and soil water storage in a small agricultural catchment. Soil and Water Research, 18: 246–268.

Liu Z. (2022): Accuracy of five ground heat flux empirical simulation methods in the surface-energy-balance-based remote-sensing evapotranspiration models. Hydrology and Earth System Sciences, 26: 6207–6226.

Monteith J.L. (1965): Evaporation and environment. In: Thornthwaite G.W. (ed.): Climatology. Symposia of the Society for Experimental Biology. Drexel Institute of Technology: 205–234.

Ochsner T.E., Sauer T.J., Horton R. (2006): Field tests of the soil heat flux plate method and some alternatives. Agronomy Journal, 98: 1005–1014.

Purdy A.J., Fisher J.B., Goulden M.L., Famiglietti J.S. (2016): Ground heat flux: An analytical review of 6 models evaluated at 88 sites and globally. Journal of Geophysical Research: Biogeosciences, 121: 3045–3059.

Sauer T.J., Norman J.M. (1995): Simulated canopy microclimate using estimated below-canopy soil surface transfer coefficients. Agricultural and Forest Meteorology, 75: 135–160.

Seguin B., Itier B. (1983): Using midday surface temperature to estimate daily evaporation from satellite thermal IR data. International Journal of Remote Sensing, 4: 371–383.

Smith K.A., Ball T., Conen F., Dobbie K.E., Massheder J., Rey A. (2018): Exchange of greenhouse gases between soil and atmosphere: Interactions of soil physical factors and biological processes. European Journal of Soil Science, 69: 10–20.

Sun M.-Y., Shi B., Cui Y.-J., Tang C.-S., Zheng X., Zhong P., Wang Y.-Q., Tong Y.-P. (2022): Evaluating three measurement methods of soil ground heat flux based on actively heated distributed temperature sensing technology. Engineering Geology, 303: 106649.

Tasumi M., Trezza R., Allen R.G., Wright J.L. (2005): Operational aspects of satellite-based energy balance models for irrigated crops in the semi-arid U.S. Irrigation and Drainage Systems, 19: 355–376.

Zawilski B.M. (2022): The soil heat flux sensor functioning checks, imbalances' origins, and forgotten energies. Geoscientific Instrumentation, Methods and Data Systems Discussions, 11: 223–234.

Received: March 10, 2025
Accepted: September 4, 2025
Published online: October 1, 2025